IIETA International Information and Engineering Technology Association
Advancing the World of Information and Engineering

Annales de Chimie - Science des Matériaux
Vol. 49, No. 5, October, 2025, pp. 531-540
Journal homepage: http://iieta.org/journals/acsm

Electrochemical Synthesis of SnO_2/Al_2O_3 Nanocomposite: Characterization and Antibacterial Activity Study

Hayder Khudhair Khattar[1*], Athmar Ali Kadhim[1], Emad Abbas Jaffar Al-Mulla[1,2]

[1] College of Health and Medical Techniques, Al-Furat Al-Awsat Technical University, An-Najaf 54001, Iraq
[2] College of Medical Technology, The Islamic University, An-Najaf 54001, Iraq

Corresponding Author Email: haider.khattarckm11@atu.edu.iq

https://doi.org/10.18280/acsm.490509

Received: 16 September 2025
Revised: 17 October 2025
Accepted: 25 October 2025
Available online: 31 October 2025

Keywords:
electrochemical, SnO_2/Al_2O_3 nanocomposite 1:1 ratio, antibacterial activity

ABSTRACT

A simple electrochemical method was used to synthesize an SnO_2/Al_2O_3 nanocomposite with a 1:1 ratio, by varying the size of the anode and examining the product using EDX analysis. This nanocomposite was then subsequently calcined at 200°C to remove impurities and achieve a homogeneous crystal structure. The SnO_2/Al_2O_3 nanocomposite was synthesized using a surfactant (PVA) as a stabilizer in the electrodeposition method and characterized using techniques. X-ray diffraction (XRD) confirmed the crystalline phases with an average crystallite size of 28 nm, while field emission scanning electron microscopy (FESEM) revealed uniform nanoparticles with an average size 21-37 nm. High-resolution transmission electron microscopy (HRTEM) average size 20 nm, (UV-Vis) spectroscopy indicated a direct band gap in the range of 3.6 eV. The anti-bacterial activity of SnO_2/Al_2O_3 nanocomposite was also evaluated against Gram-positive Staphylococcus aureus and Streptococcus mutans, as well as Gram-negative Escherichia coli and Proteus mirabilis. the inhibition zone diameters increased with concentration from 10-1000 ppm, reaching 23 nm for *S. aureus* and 24 nm for *Str. mutans* at 1000 ppm, while *E. coli* and *P. mirabilis* reached 17 nm and 16 nm, respectively. these results show that SnO_2/Al_2O_3 nanocomposite possesses structural, optical, and antibacterial properties, making it a suitable candidate for applications in electronics, optoelectronics, and antimicrobial coating.

1. INTRODUCTION

Semiconductor metal oxides in nanocrystals differ in their behavior from the bulk states such as Al_2O_3, and SnO_2. Because of the importance of these materials in multiple applications such as sensors, optoelectronic devices, solar cells, and thin-film transistors, their properties have been extensively studied [1, 2]. Nanometal oxides and their composites are well-known for their structural and high optical transmittance in the UV-Vis region and high IR reflectance [3-6]. The structural and visual properties are improved by relying on composition and size, as well as on the superficial area of nanoparticles. Therefore, the composite of hard nanostructured materials, such as SnO_2 and Al_2O_3. It may be promising to produce excellent nanocomposites, there are many methods for synthesizing NPs, such as chemical vapor deposition [7], solvothermal methods [8], and microemulsion methods [9]. Sol-gel: this wet chemical technique involves converting precursors into a gel, which is then dried and sintered to form the desired nanomaterial. While relatively simple, it can require long processing times and the use of surfactants or stabilizers [10]. Laser ablation: this technique uses a laser to vaporize a target material, creating nanoparticles in a liquid medium. It can produce high-quality nanoparticles, however, the equipment can be expensive, and scaling up production can be challenging [11]. Hydrothermal methods utilizing high-pressure and high-temperature water for chemical reactions can be effective for synthesizing SnO_2/Al_2O_3 materials, often require complex setups and specific conditions. The process depends on the solubility of reactants in water under elevated temperatures and pressures within a closed vessel. Among the most prominent limitations is the difficulty of ensuring a homogeneous nanodistribution of the two different SnO_2-Al_2O_3 phases within the compound, which leads to aggregation of particles or a decrease in the effectiveness of the reaction; the need for high temperatures or pressures or the use of expensive chemicals or harmful solvents; the slow process of synthesis or the inability to effectively expand industrially; weakness in controlling the fine nanostructure and controlling the size of particles and pores, which reduces the antibacterial or photocatalytic effectiveness [12]. The use of electrochemical deposition technology has emerged as a promising option to overcome these limitations due to the better control it provides over the distribution of the nanophase and the formation of a homogeneous film layer on the substrate or in the liquid; the possibility of performing synthesis at lower temperatures and with relatively simple equipment, which reduces the cost and facilitates expansion; greater speed in the formation and growth of particles with the possibility of adjusting the current

density, voltage, time, and solvent to obtain a controlled particle size; and the opportunity To obtain more contact interfaces between the SnO_2-Al_2O_3, which may improve the antibacterial properties through greater surface activation or improved charge transfer. Through the data, the need has been to find a way through which effective and low-cost, as well as developmental and environmental, electrodeposition is a process that enables the formation of solid deposits on the surface of the electrically connected materials. It involves coating the surface of an electrode with a thin layer of the desired material. Electroplating employs an electric current to reduce dissolved metal cations in solution, forming a thin coating on the surface of the electrode. These deposits are produced using electrochemical cells, which consist of two conductors or semiconductors [13]. The electrochemical deposition mechanism involves immersing electrodes of the desired metal in a solution containing strong electrolyte ions, then applying an electric voltage or current that causes the ions to move toward the corresponding electrodes, where they undergo reduction and oxidation reactions. The anode electrode undergoing electrolysis is deposited in the middle of the solution by adjusting parameters such as voltage or current, deposition time, and ion concentration, where the size and shape of the particles can be controlled. However, this technique is rarely used in the preparation of SnO_2/Al_2O_3 nanocomposites. And evaluate its antibacterial effectiveness, which constitutes a research gap that this study seeks to fill by preparing the compound by electrochemical deposition, characterizing it, and evaluating its antibacterial activity. This study focuses on the synthesis of SnO_2/Al_2O_3 nanocomposite using an effective and surfactant-free electrodeposition method. The research aims to take advantage of the priority of electrical expression, such as the exact control of the thickness of the film, uniformity, and formation to produce these nanoparticles. The study will investigate the structural and optical properties of the synthesized nanocomposite, with the aim of exploring their potential applications in electronics, optoelectronics and sensor technologies, and antibacterial properties. The advantages of electrodeposition include its low cost, low energy consumption, environmentally friendly nature, reduced material waste, and the ability to produce thin films at low temperatures. The film formation process and fundamental properties can be controlled by adjusting the applied potential [14]. This study aims to prepare SnO_2/Al_2O_3 nanocomposite by electrophoretic deposition technique, describe its compositional, morphological, and surface properties, and then evaluate its antibacterial effectiveness. To achieve this by preparing nanoparticles or SnO_2-Al_2O_3 layers by controlling electrochemical deposition parameters such as voltage, current, time, and ion concentration, and analyzing the crystalline structure, shape, and phase distribution of the compound using techniques such as UV, FTIR, XRD, FESEM, EDX, and HRTEM; evaluating the antibacterial activity of the prepared compound against selected strains; and studying the effect of the concentration of the prepared nanocomposite.

2. EXPERIMENT

2.1 Materials and methods

The electrical system for preparing Nanocomposites SnO_2/Al_2O_3 using a glass cell with a capacity of 100 ml and using the positive electrode, (anode), which is an Aluminum plate with an area of 2 cm^2 (99%, Aldrich), as well as the Tin electrode 99% purity, with an area of 2cm (99%, Aldrich), the cathode negative electrode, which is graphite with an area of 4 cm, and the electrical current preparation The device used in the operation, is (5000 milli-ampere mA) maximum currents and 30 volts (V) maximum voltage, China) used in this method as a magnetic stirrer to mix the materials by stirring. Wash the poles used in this method with ethanol, then with deionized water, to remove the stranded organic materials. Add about 1 gram of a strong electrolyte material like KCL (99% Thomas, Indi). And 10 mL of 1g/100 mL of the stabilizer (Polyvinyl alcohol (PVA CDH-India), and deionized water, net foil of Al-Sn (4 cm × 2 cm × 0.25 mm) for every, inert graphite electrode (4 cm × 2 cm) was utilized as anode and cathode respectively, as shown in Table 1, They are positioned facing each other in the electric cell solution with a depth of 2 cm for both. The electric cell was operating for one hour for 40 to 50°C, It was centrifuged through a centrifugal device, The sediments were washed with deionized water and ethanol three times and dried at a temperature of 60°C for one hour and after that, the sediments have then calcined in an oven at 200°C for 2 hours, SnO_2/Al_2O_3 composites were characterized by EDS, XRD, FESEM, HRTEM.

Table 1. The experimental data account for the EDS measurements

	Chemicals		EDX
	0.1 g/100 ml	KCL (99% Thomas, Indi)	
	0.5 g/100 ml	KOH (99% Thomas, Indi)	
	1g/100 mL. We take 10 ml	PVA (CDH-India)	
	0.7 µS/cm	Deionizedwater	
	10-12	pH	
	40-50°C	Temperature	
	500 mA/m^2	Current density	
1	24 cm^2	Al (2 cm^2)/Sn (2 cm^2) Anode area	Al = 27.24 Sn = 31.89 (Atomic % ratio = 1:1.17) O = 40.87
	24 cm^2	Graphite cathode	
	0.75-1.2 A	Current density	
	7-15 V/60 (min)	Voltage/time	
2	18 cm^2	Al (2 cm^2)/Sn (1 cm^2) Anode area	Al = 22.47 Sn = 43.65 (Atomic % ratio = 1:1.44) O = 47.01
	24 cm^2	Graphite cathode	
	0.75-1.2 A	Current density	
	11-15 V/60 (min)	Voltage/time	
3	15 cm^2	Al (2 cm^2)/Sn (0.5 cm^2) Anode area	Al = 31.34 Sn = 21.84 (Atomic % ratio = 1:1.95) O = 33.70
	24 cm^2	Graphite cathode	
	0.36-1.2 A	Current density	

	10-15 V/60 (min)	Voltage/time	
	18 cm^2	Al (1 cm^2)/Sn (2 cm^2) Anode area	
	24 cm^2	Graphite cathode	Al = 30.68
4	0.35 -1.2 A	Current density	Sn = 23.31 (Atomic % ratio = 1:1.31)
	7-15 V/60 (min)	Voltage/time	O = 46.01
	24 cm^2	Al (2 cm^2)/Sn (2 cm^2) Anode area	
	15 cm^2	Al (0.5 cm^2)/Sn (2 cm^2) Anode area	
	24 cm^2	Graphite cathode	Al = 28.67
5	0.75 -1.2 A	Current density	Sn = 28.32 (Atomic % ratio = 1:1.01)
	7-15 V/60 (min)	Voltage/time	O = 43.01

2.2 Synthesis of SnO_2/Al_2O_3 nanocomposite (1:1 ratio)

The basis for the procedure is to control the size of SnO_2 and Al_2O_3 nanoparticles by adjusting the size of the electrodes used, especially the positive electrode anode, Al (2 cm^2) and Sn (1 cm^2), with an total anode area of 24 cm^2 two faces, opposite graphite cathode 24 cm^2, in the first experiment, we used two poles of equal size, and the result, according to Energy Dispersive X-Ray Spectroscopy (EDX) analysis (BRUKER) of the granules, was 1:1.17 atomic%. KCL, KOH, deionized water, and the PVA stabilizer were also used as the electrolyte. In the second experiment, the Sn and the Al poles were prepared with the required dimensions before the process, Al (2 cm^2) and Sn (1 cm^2), giving an anode area of 18 cm^2, opposite a graphite cathode 24 cm^2. The grain size ratio from EDX was 1:1.44 atomic%, as shown in Table 1. The change in this experiment involved only the anode size, while all other parameters remained fixed. In the third experiment, the tin pole area was 0.5 cm^2 and the aluminum electrode area was 2 cm^2, resulting in an EDX atomic% ratio for SnO_2/Al_2O_3 of 1:1.95. In the fourth experiment, the tin pole size was 2 cm^2 and the aluminum electrode size was 1 cm^2, resulting in an EDX atomic% ratio of SnO_2/Al_2O_3 was 1:1.31. The best result was obtained in the fifth experiment, using a tin pole area of 2 cm^2 and an aluminum electrode size 0.5cm^2, yielding an EDX atomic% ratio for SnO_2/Al_2O_3 of 1:1.01. This ratio is considered the most optimal among the tested configurations and could be applied in various industrial and biological fields.

3. RESULTS AND DISCUSSION

3.1 X-Ray Diffraction

The XRD patterns of the SnO_2/Al_2O_3 nanocomposites are shown in Figure 1. The miller indices (hkl) of the diffraction peaks of SnO_2/Al_2O_3 and nanocomposites were matched with JCPDS cards No. 71-1123 and No. 41-1445. The crystallite size was calculated using the Scherer formula [15, 16]. where D is the average crystallite size, λ is the used X-ray wavelength and k = 0.94 is a constant, θ is the diffraction angle (in degrees), and β is the full width at half maximum (FWHM, in radians) of the observed diffraction peak [17]. The XRD pattern of SnO_2/Al_2O_3 in Figure 1 shows low peaks at 2θ values of 25.12°, 43.80°, and 57.60°, which correspond Al_2O_3 phase and confirm the presence of Al_2O_3 in the composite. Three intense diffraction peaks at 27.38°, 39.57°, and 49.24° can be attributed to the (110), (200), and (211) planes of SnO_2, respectively. Compared with pure SnO_2, the peaks near 27.38° in the SnO_2/Al_2O_3 composites appear broader, which may be due to the overlap of the SnO_2 (110) and Al_2O_3 (012) peaks [18, 19]. The tabulated X-ray data include: 2-Theta (diffraction angle), d (nm) (interplanar spacing), BG (background), height (peak intensity), I% (relative intensity), area (integrated peak intensity), I%$_2$ (another relative intensity), full width at half maximum (FWHM), and crystal size (nm). The crystal size, calculated using the Scherrer equation, was approximately 11.13 nm as shown in Table 2.

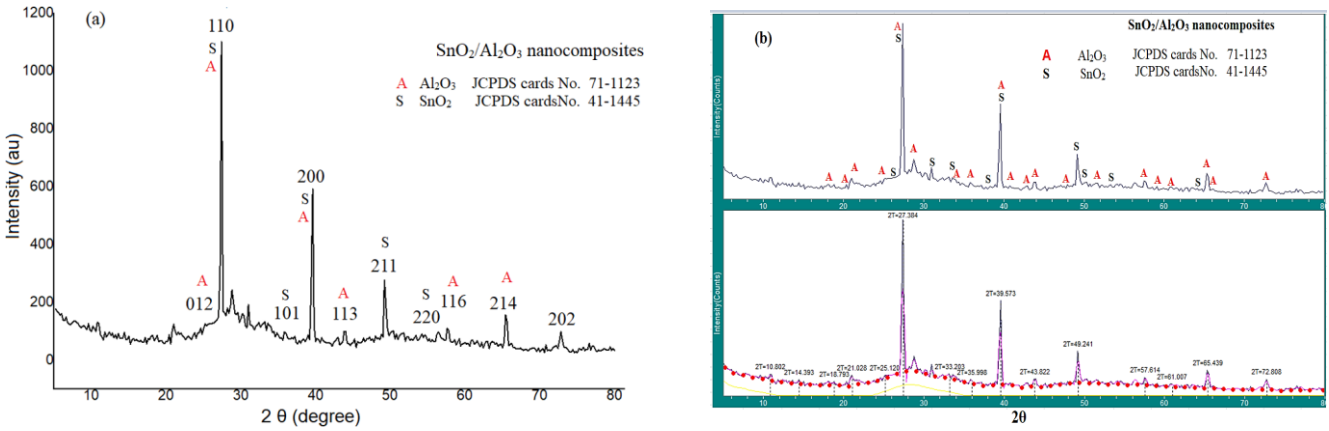

Figure 1. XRD Pattern of SnO_2/Al_2O_3 nanocomposites (a) Miller Indices (hkl), (b) Two-theta (2θ) represent angles related to the diffraction of X-rays by a crystalline sample

Table 2. The data obtained from X-ray diffraction (XRD)

2-Theta	D (nm)	BG	Height	I%	Area	I%$_2$	FWHM	Crystal Size (nm)
10.802	0.81839	7	124	11.9	857	42.3	1.175	7
14.393	0.61487	0	96	9.2	776	38.3	1.374	6
18.793	0.47179	0	86	8.3	547	27	1.081	8
21.028	0.42213	0	124	11.9	833	41.1	1.142	7
25.12	0.35421	23	103	9.9	701	34.6	1.157	7

27.384	0.32542	60	1041	100	2027	100	0.331	28
33.203	0.2696	18	115	11	919	45.3	1.359	6
35.998	0.24928	0	95	9.1	489	24.1	0.875	10
39.573	0.22755	0	592	56.9	1528	75.4	0.439	21
43.822	0.20642	0	100	9.6	543	26.8	0.923	10
49.241	0.18489	0	277	26.6	906	44.7	0.556	17
57.614	0.15985	0	111	10.7	669	33	1.025	9
61.007	0.15175	0	69	6.6	470	23.2	1.158	8
65.439	0.14251	0	157	15.1	652	32.2	0.706	14
72.808	0.12979	0	99	9.5	653	32.2	1.121	9

3.2 UV-Vis spectrum

The UV-Vis spectra were analyzed to investigate the optical properties. The compounds and their absorbance changes are shown in Figure 2(a). The SnO_2/Al_2O_3 nanocomposites exhibit strong absorption at 200 nm, with the absorption decreasing slightly as the wavelength increases. In the UV-visible range, no distinct peak was observed in the long wavelength region. Moreover, the maximum absorption was detected at about 235 nm, after which the absorbance gradually decreased [20]. The UV−Vis diffuse reflectance spectra display the results for the SnO_2/Al_2O_3 samples in the range of 200-700 nm. The results showed that the absorption edge of the SnO_2/Al_2O_3 nanocomposite occurred at 310 nm, which is in good agreement with the value (298 nm) reported by Mishra et al. [5] for SnO_2-Al_2O_3 composites prepared via the sol−gel method. From the reflection spectra, the bandgap energy (Eg), was determined using a Tauc plot. In this method, $(\alpha h\nu)^{1/2}$(eV. $cm^{-1})^{1/2}$ is plotted against hν, where α is the absorption coefficient, h is Planck's constant, ν is the photon frequency, and γ depends on the type of electronic transition (e.g., 1/2 for indirect transition, 2 for direct transition). Extrapolating the linear portion of the curve to the x-axis (energy axis) gives the band gap energy, as shown in the inset of Figure 2(b). The bandgap values are found to be 3.65 eV for the SnO_2/Al_2O_3 nanocomposite [21].

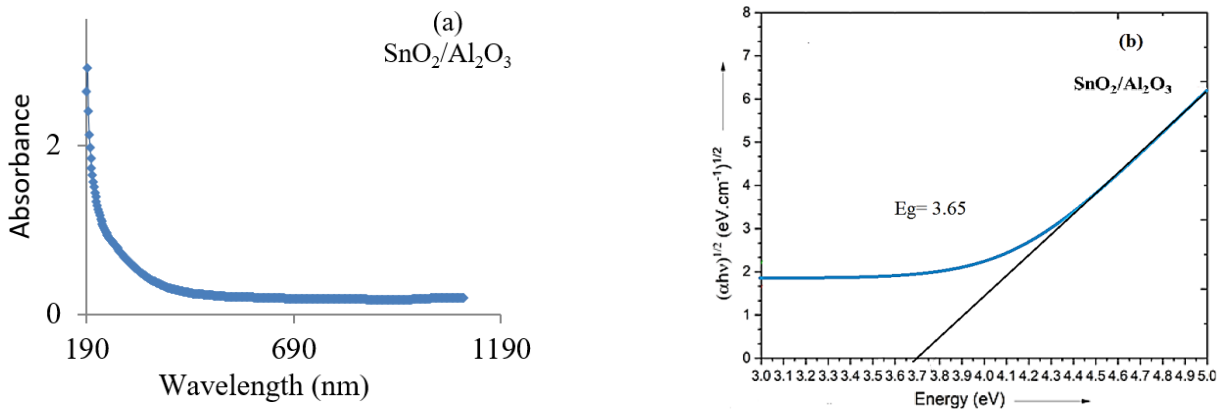

Figure 2. (a) UV–Vis Spectra, (b) the plot of $(\alpha h\nu)^{1/2}$ vs. photon energy ($h\nu$) for SnO_2/Al_2O_3 nanocomposites

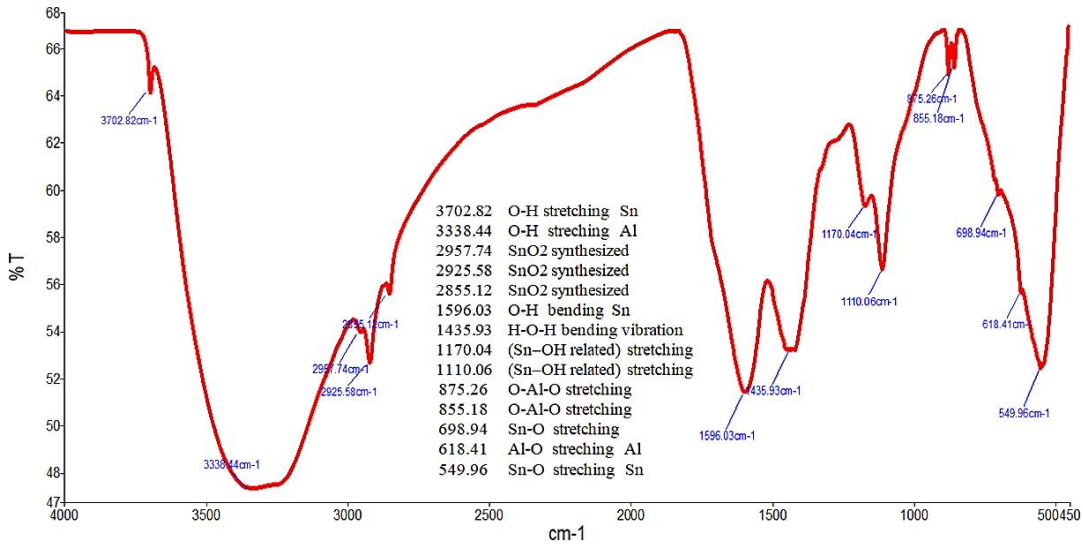

Figure 3. FTIR spectrum of the SnO_2/Al_2O_3 nanocomposites

3.3 FTIR analysis of 1:1 SnO_2/Al_2O_3 nanocomposites

For important information about functional groups in SnO_2/Al_2O_3, FTIR spectra are recorded in transmission mode. FTIR spectra are shown in Figure 3. The broad peak at around 3200 cm^{-1} can be attributed to the O-H. It is noted that the lowest is in SnO_2/Al_2O_3. Moreover, the bending vibrations of the O-H stretching vibration. It is noted that this peak is less

intense in SNO_2/Al_2O_3. Moreover, the bending vibrations of the O-H group are responsible for the peaks at about 1630 cm^{-1} in SnO_2/Al_2O_3 nanocomposites [22]. The peak at about 500 cm^{-1} in SnO_2/Al_2O_3 nanocomposites can be assigned to Sn-O or O-Sn-O vibrations [23]. The intensity of this peak decreases significantly for SnO_2/Al_2O_3 nanocomposites, as shown in Figure 3. This decrease in metal-oxygen vibrations can be attributed to Sn or O vacancies in SnO_2/Al_2O_3 powder. Similarly, the peaks at about 650 cm^{-1}, 1100 cm^{-1}, and 1450 cm^{-1} in SnO_2/Al_2O_3 nanocomposites are mostly due to Al-O and O-Al-O vibrations as in Table 3 [24]. The disappearance or reduction of Al or O atom can lead to a decrease in the strength of these peaks. The absence of Sn, Al or O may result in weaker metal-oxygen stretching in the SnO_2/Al_2O_3 bonding. The broadening of these peaks in the SnO_2/Al_2O_3 powder suggests the presence of multiple weak vibrations instead of one strong vibration [22, 23]. From the FTIR spectrum, it is evident that the SnO_2/Al_2O_3 powder contains a significant number of Sn, Al or O vacancies. However, these vacancies are relatively few compared to what might be expected, likely due to the absence of severe metal-oxygen loss during high-temperature calcination. Since the powder was dried in a hot air oven at 200°C in an oxygen-adequate environment, the possibility of O vacancies is minimized. Furthermore, in SnO_2/Al_2O_3 powder, the reduction of peak intensities related to metal-oxygen vibrations supports the presence of such lattice defects.

Table 3. FTIR vibration bands and their corresponding bond assignments for the SnO_2/Al_2O_3 nanocomposite

Wavenumber (cm^{-1})	Bond / Functional Group	Comment	Reference
3500–3400	O–H stretching (surface hydroxyl groups, adsorbed moisture)	Broad peak due to hydrogen-bonded OH groups	[25, 26]
3240–3435	O–H stretching (alcohol/water)	Strong hydrogen bonding in surface hydroxyls	[25]
1630–1640	H–O–H bending vibration	Bending mode of adsorbed water molecules	[26]
605 and 480	Sn–O and Sn–O–Sn stretching,	Asymmetric and symmetric	[27]
3400, 2925, 2851 and 1636	SnO_2 synthesized	Indicating the presence of extract molecules in the SnO_2 synthesized	[27]
1190–1200	C=O stretching (Sn–OH related)	Surface hydroxyl-carbonyl-like vibrations	[28]
860–820	O–Al–O stretching	Al_2O_3 lattice vibrations	[29]
620–600	Sn–O and Sn=O stretching	Characteristic of SnO_2	[30]
560–500	O–Al–O bending / Sn–O–Sn symmetric stretching	Evidence of mixed oxide bonding	[29, 30]

3.4 FESEM, RHTEM, and EDX

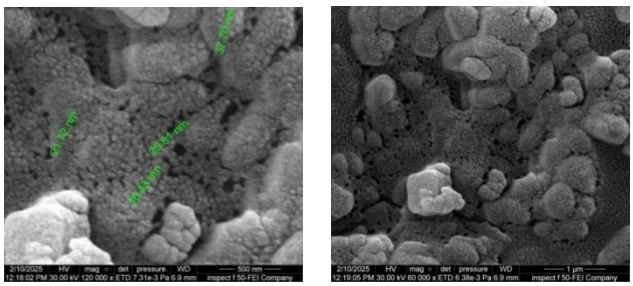

Figure 4. FESEM micrograph of SnO_2/Al_2O_3 nanocomposite

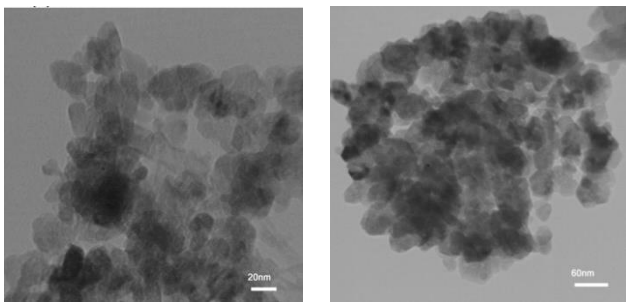

Figure 5. HRTEM micrograph of SnO_2/Al_2O_3 nanocomposite

Figure 4 shows the field emission scanning electron microscopy (FESEM) image of SnO_2/Al_2O_3 nanocomposite particles in various size ranges up to 500 nm. The microscopic image reveals that the nanocomposites tend to aggregate on the surface, confirming the presence of pores, which can be useful in sensing applications. The particle size is approximately 21-37 nm, which is larger than that calculated from XRD analysis [31]. Figure 5 shows high-resolution transmission electron microscopy (HR-TEM) images of the SnO_2/Al_2O_3 nanocomposite. HRTIM analysis is among the most effective methods to investigate nanoparticle size. The practical size in this work was found to be around 20 nm. The images also show that the grain size distribution is not uniform. During sample preparation, agglomeration of particles may occur. Energy dispersive X-ray (EDX) spectroscopy of the SnO_2/Al_2O_3 nanocomposite confirms the presence of its constituent elements. Energy-Dispersive For the 1:1 sample (Experiment 5), the mass composition was O = 43.01%, Al = 28.67% and Sn = 28.32%. Also, maps with a resolution of 768 × 512 were obtained to ensure racial distribution. These results confirm the expected chemical structure of the SnO_2/Al_2O_3 compound, and show good agreement with X-Ray Diffraction (XRD) data, as in Figure 6 [32, 33].

The average particle size of SnO_2/Al_2O_3 nanoparticles, as determined by XRD, FE-SEM, and HRTEM analyses, showed a good agreement through the three characterization techniques, with minor differences attributed to the related differences in the principles of measurement. The XRD-derived size, calculated using the Scherrer equation, reflects the average size of crystals, and that may be a little smaller than the size of the particles observed in the FESEM and HRTEM images due to the potential assembly and the polycrystal nature of the particle. FESEM analysis presented a direct visualization of particle morphology. This reveals a structure with agglomeration and uniform particles with a small mass. HRTEM has provided high-resolution images, allowing an accurate measurement of individual molecules and confirming the crystallinity of the lattice corresponding to SnO_2 and Al_2O_3, when compared to the values mentioned in the literature shown in the Table 4, the sizes of the particles

obtained within the expected range of XRD were within the expected range of 11.13 nm, in line with pre-reported studies [5, 34-37]. Slight deviations from literature data may result from differences in the terms of synthesis, base materials, calcination temperatures, and SnO_2 to Al_2O_3 ratios. This indicates that the approved synthesis method produces effectively from nanoparticles of similar particles, or smaller than those that have been previously reported, which can enhance the surface area and catalytic activity.

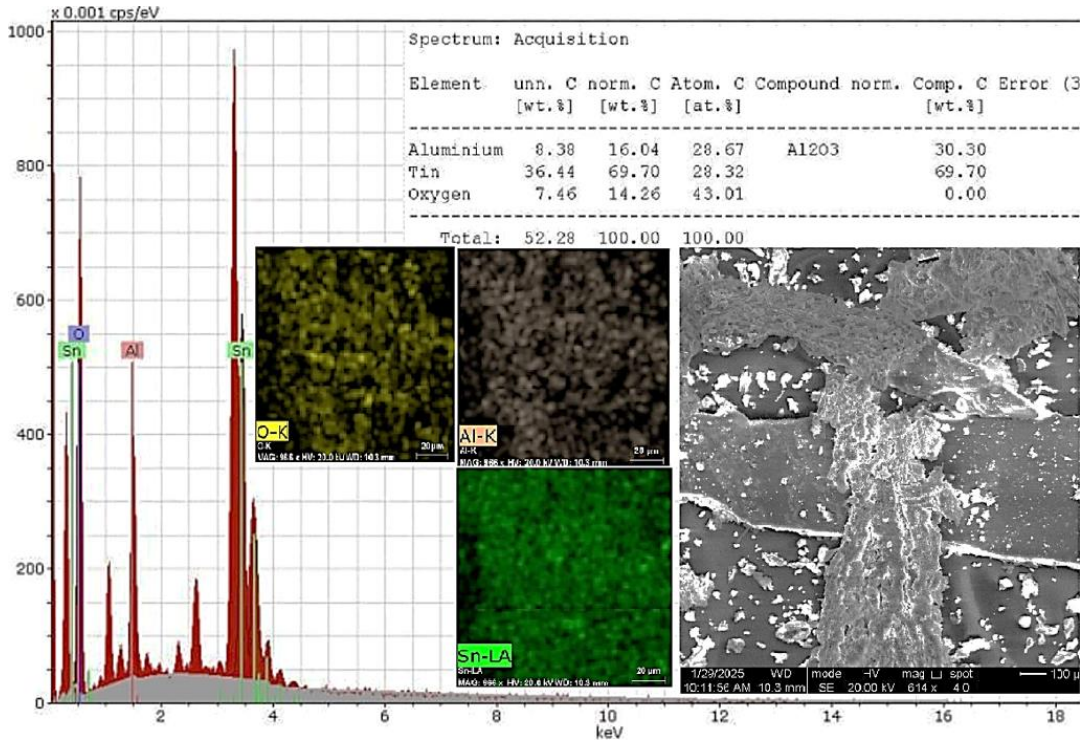

Figure 6. Energy dispersive X-ray (EDX) spectroscopic analysis of SnO_2/Al_2O_3 nanocomposite showing Al=28.67 atomic%, Sn =28.32 atomic%, O = 43.01 atomic%

Table 4. Comparing the average particle size of the SnO_2/Al_2O_3 nanoparticles calculated by XRD, FESEM, and HR-TEM techniques with reported literature values

Size Technique	Size (nm)	Shape/Surface	Reported Values in Literature (nm)	Literature Reference
XRD	11.13	Derived from Scherrer equation	13-15 12.1	[34] [37] [5]
FESEM	21-37	Morphology observation	62	[5]
HRTEM	20-60	Detailed shape and boundary analysis	20-25, 30 20-80 5-100	[35] [36] [37]

4. ANTIBACTERIAL ACTIVITY USING AGAR ROUT

The in vitro antibacterial activity of the compound was evaluated against *Staphylococcus Aureus*, *Streptococcus mutans*, *Escherichia coli*, and *Proteus mirabilis* using the well-diffusion method on Muller-Hinton agar (7). Wells of 6 mm in diameter were made in the agar plates using a sterile cork borer. The agar surfaces were then inoculated with each bacterial strain. The synthesized SnO_2/Al_2O_3 nanocomposite particles were dissolved in dimethylformamide (DMF) to prepare solutions with concentrations of 10, 100, and 1000 ppm. The plates were incubated at 37°C for 12 hours, and the inhibition zones were measured in millimeters. Each test was performed in triplicate, and the average inhibition zone's diameter was recorded.

4.1 Antibacterial activity studies

Semiconductors or metal oxides are among the promising alternatives for antibacterial application. after incubation, the wells loaded with SnO_2/Al_2O_3 nanocomposite showed bactericidal activity against *E. coli* and *P. aeruginosa*, comparable to Ciprofloxacin (used as the standard), as evidenced by the inhibition zones. The antibacterial capacity is strongly influenced by the morphology of nanoparticles. Smaller nanoparticles are generally preferred few sizes, these nanoparticles are preferred because of their potent bactericidal effects. Several reports indicate that nanoparticles in contact with bacterial walls can inhibit the synthesis of sulfur or phosphorus-containing envelope proteins. When the DNA interacts with metal oxide ions, the Al^{+3} and Sn^{+2} ions may induce biochemical changes that ultimately lead to cell death. This may involve interference with the electron transport chain (ETC), disruption of ion pumps alteration of ion movement across the membrane [38]. Weakening of the bacterial plasma membrane can further stimulate cell death. Overall, the tested microorganism was not resistant and did not display any

biofilm formation in response to the synthesized nanoparticles. These findings are consistent with previous studies, supporting the bactericidal potential of Al_2O_3 and SnO_2 nanoparticles.

Table 5. Antibacterial activity of SnO_2/Al_2O_3 at various concentrations, expressed as the zone of inhibition mm

Concentration SnO_2/Al_2O_3	G(+Ve)		G(-Ve)	
	S. aureus	*Str. mutans*	*E. coli*	*P. mirabilis*
10 ppm	12	15	7	9
100 ppm	17	20	14	12
1000 ppm	23	24	17	16

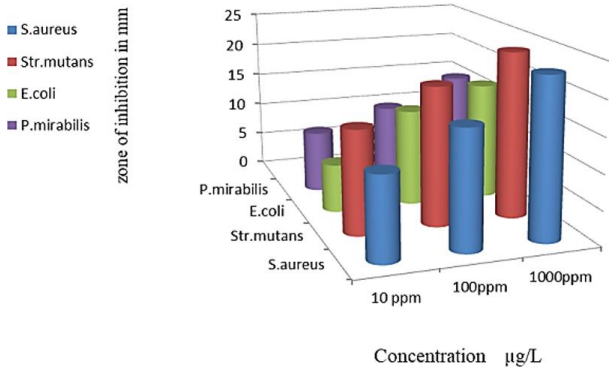

Figure 7. Statistical representation of antibacterial activity of SnO_2/ Al_2O_3

The biological activity of the (SnO_2/Al_2O_3) nanocomposite was evaluated in vitro against *S. aureus, Str. mutans, E. coli, and mirabilis* using the well-diffusion method. The inhibition zones for each bacterial strain are presented in Table 5, with statistical analysis is shown in Figure 7. The results indicate that the (SnO_2/Al_2O_3) Gram-positive bacteria has a stronger effect on the Gram-positive bacteria (*S. aureus, Str. mutans*) than on the Gram-negative strains tested, under identical experimental conditions. At concentrations of 10 and 100 ppm, the nanocomposite exhibited mild activity against (*S. aureus, Str. mutans*), while at 1000 ppm it showed high antibacterial potency. In contrast, its activity against *E. coli* and *P. mirabilis* was moderate to weak at 10 and 100 ppm, and moderate at 1000 ppm. The inhibition effect at the concentration of 1000 ppm was moderate. These findings are consistent with previous reports [39], which also observed higher inhibition of Gram-positive bacteria compared to Gram-negative bacteria, despite the thicker peptidoglycan layer of Gram-positive. This difference is likely due to the outer membrane of Gram-negative bacteria, which acts as an additional barrier to nanoparticle penetration [40]. The results in Table 5 further support this, showing greater efficacy against the Gram-positive strains. This can be explained by structural differences in the bacterial cell envelope gram-negative bacteria possess an extra outer membrane in addition to the peptidoglycan layer, creating an additional barrier that limits biocide penetration [41].

4.2 The experimental determination of the minimum inhibitory concentration (MIC) for antibacterial activity

As shown in Table 6, these results provide evidence that the nanocomposite SnO_2/Al_2O_3 has inhibitory effects against the studied bacterial strains, *Staphylococcus aureus and Streptococcus mutans,* were inhibited at a concentration of 10 ppm, whereas *Escherichia coli and Proteus mirabilis* were inhibited at a concentration of 100 ppm. Thus, the results confirm that Gram-negative bacteria are approximately ten times less sensitive than Gram-positive bacteria [42, 43].

Table 6. Shows the results of the minimum inhibitory Concentration (MIC) of the SnO_2/Al_2O_3 nanocomposite

MIC (ppm)	Bacterial Strain
10	*Staphlococcus aureus* (*S. aureus*)
10	*Streptococcus mutans (Str. mutans)*
100	*Escherichia coli* (*E. coli*)
100	*Proteus mirabilis* (*P. mirabilis*)

4.3 Antibacterial activity inhibition mechanism by SnO_2/Al_2O_3 nanocomposite

The low sensitivity of Gram-negative bacteria is likely due, at least in part, to the limited absorption of nanoparticles and to differences in the structure of the cell wall, an outer layer of lipopolysaccharide (LPS) reduces the permeability of nanoparticles [44-46]. As for the antibacterial behavior of the SnO_2/Al_2O_3 nanocomposite, several mechanisms are involved, including the generation of reactive oxygen species (ROS), which leads to the formation of a matrix that directly damages the cellular components of bacteria [37, 43, 44, 46]. Evidence indicates that the cell membrane was compromised, likely through direct interaction with the cell surface [43, 44], leading to the release of active ions that interfered with essential bacterial processes such as iron siderophore absorption [45, 46]. Therefore, the SnO_2/Al_2O_3 nanocomposite could have practical applications in the medical and dental fields, such as antibacterial coatings for medical devices and oral care products [42, 47, 48]. It should be noted that Gram-negative bacteria exhibit relative resistance to this compound, indicating the need for targeted strategies to enhance its antibacterial efficacy.

5. CONCLUSION

Using the simple electrical method, the SnO_2/Al_2O_3 nanocomposite was prepared. The crystal size and the morphology of the sample, analyzed via X-ray diffraction and several different techniques, indicate the products crystallinity, crystallite size, and other characteristic properties, signaling that the utilized process is proper and economical for obtaining SnO_2/Al_2O_3 nanocomposites. It can be stated that SnO_2/Al_2O_3 at a concentration of (1000) ppm can act as powerful antibiotics agent with potential effects on other bacteria types not yet tested. However, SnO_2/Al_2O_3 may not show a similar effect in vivo despite the bacteria sensitivity observed in vitro, as in vivo conditions often differ significantly. Therapeutic process involves complex metabolic and physiological reactions that are difficult to estimate despite knowing the final treatment outcomes, whether positive or negative. Additionally, other factors may interfere with antibiotic efficacy, resulting in outcomes that are difficult to explain. It was observed that the Gram-positive bacteria are inhibited by relatively low concentration of the nanocomposite, whereas Gram-negative bacteria require much higher concentration for inhibition. The difference in sensitivity is due to variations in the general structure of the bacterial cell wall, with each bacterial type requiring a specific compound for effective inhibition. The nanocomposite has

shown an additional advantage: antibacterial activity against antibiotic-resistant strains due to the multiple mechanisms, including increasing ROS generation, membrane disruption, and ion release. The nanocomposite can be used in many fields, such as antibacterial coatings and medical devices. It may also be applied in further studies, such as surface property modifications to improve its efficacy against Gram-negative bacteria. SnO_2/Al_2O_3 nanocomposite, a semiconductor with controlled capacity and porosity, has multiple enforcement possibilities and also has work in the industrial field. SnO_2 is supported by a stable Al_2O_3 core. This feature makes it suitable for fields such as gas sensors or catalytic materials. For example, a similar version has been studied for detecting low-concentration gases using small-sized oxides. At the environmental/biological level, preliminary studies have shown the antibacterial effectiveness of nano-metal oxides, including alumina, which opens up to use in sterilization or antimicrobial materials. Therefore, our study, which focuses on the synthesis of SnO_2/Al_2O_3 via electrochemical deposition, is not just an addition to knowledge but rather paves the way for potential applications in environmental and health sensors, that is, in a series linking nanopreparation and functional improvement.

REFERENCES

[1] Shah, N.A., Gul, M., Abbas, M., Amin, M. (2019). Synthesis of metal oxide semiconductor nanostructures for gas sensors. In Gas Sensors. IntechOpen. https://doi.org/10.5772/intechopen.86815

[2] Al-Abboodi, H., Fan, H., Al-Bahrani, M., Abdelhussien, A., Mohamad, B. (2024). Mechanical characteristics of nano-crystalline material in metallic glass formers. FACTA UNIVERSITATIS Series: Mechanical Engineering, 22(2): 315-328. https://doi.org/10.22190/FUME230128016A

[3] Abd-Elnaiem, A.M., Rashad, M., Hanafy, T.A., Shaalan, N.M. (2023). Improvement of optical properties of functionalized polyvinyl alcohol-zinc oxide hybrid nanocomposites for wide UV optoelectronic applications. Journal of Inorganic and Organometallic Polymers and Materials, 33(8): 2429-2444. https://doi.org/10.1007/s10904-023-02616-w

[4] Sohn, H.Y., Murali, A. (2021). Plasma synthesis of advanced metal oxide nanoparticles and their applications as transparent conducting oxide thin films. Molecules, 26(5): 1456. https://doi.org/10.3390/molecules26051456

[5] Mishra, N.K., Kumar, C., Kumar, A., Kumar, M., Chaudhary, P., Singh, R. (2015). Structural and optical properties of SnO_2–Al_2O_3 nanocomposite synthesized via sol-gel route. Materials Science-Poland, 33(4): 714-718. https://doi.org/10.1515/msp-2015-0101

[6] Chavan, G.T., Kim, Y., Khokhar, M.Q., Hussain, S.Q., et al. (2023). A brief review of transparent conducting oxides (TCO): The influence of different deposition techniques on the efficiency of solar cells. Nanomaterials, 13(7): 1226. https://doi.org/10.3390/nano13071226

[7] Wu, F., Wang, C., Hu, H.Y., Pan, M., et al. (2019). One-step synthesis of hierarchical metal oxide nanosheet/carbon nanotube composites by chemical vapor deposition. Journal of Materials Science, 54(2): 1291-1303. https://doi.org/10.1007/s10853-018-2889-9

[8] Liang, Y., Jiang, L., Xu, S., Ju, W., et al. (2024). Synthesis and characterization of Fe_3O_4 nanoparticles prepared by solvothermal method. Journal of Materials Engineering and Performance, 33(13): 6804-6815. https://doi.org/10.1007/s11665-023-08431-1

[9] Asab, G., Zereffa, E.A., Abdo Seghne, T. (2020). Synthesis of Silica-Coated Fe_3O_4 nanoparticles by microemulsion method: Characterization and evaluation of antimicrobial activity. International Journal of Biomaterials, 2020(1): 4783612. https://doi.org/10.1155/2020/4783612

[10] Patel, G.H., Chaki, S.H., Kannaujiya, R.M., Parekh, Z.R., Hirpara, A.B., Khimani, A.J., Deshpande, M.P. (2021). Sol-gel synthesis and thermal characterization of SnO_2 nanoparticles. Physica B: Condensed Matter, 613: 412987. https://doi.org/10.1016/j.physb.2021.412987

[11] Crivellaro, S., Guadagnini, A., Arboleda, D.M., Schinca, D., Amendola, V. (2019). A system for the synthesis of nanoparticles by laser ablation in liquid that is remotely controlled with PC or smartphone. Review of Scientific Instruments, 90(3): 033902. https://doi.org/10.1063/1.5083811

[12] Kafi, F.S.B., Gunaratna, B.H., Jayathilaka, K.M.D.C., Wijesundera, R.P. (2024). Electrodeposited thin film SnO_2 photoelectrode for PEC applications. Proceedings of the Technical Sessions, 40(2024): 47-53.

[13] Pelegrini, S., Brandt, I.S., Cid, C.C.P., Isoppo, E.A., Viegas, A.D., Pasa, A.A. (2015). Electrochemical Cl doping of Cu_2O: Structural and morphological properties. ECS Journal of Solid State Science and Technology, 4(7): P181. https://doi.org/10.1149/2.0041507jss

[14] Zahra, T., Alanazi, M.M., Alahmari, S.D., Abdelmohsen, S.A., et al. (2024). Hydrothermally synthesized ZnSe@ FeSe nanocomposite: A promising candidate for energy storage devices. International Journal of Hydrogen Energy, 59: 97-106. https://doi.org/10.1016/j.ijhydene.2024.01.293

[15] Kumar, S., Mote, V.D., Prakash, R., Kumar, V. (2016). X-ray analysis of α-Al_2O_3 particles by Williamson–Hall methods. Materials Focus, 5(6): 545-549. https://doi.org/10.1166/mat.2016.1345

[16] Nagarani, S., Sasikala, G., Satheesh, K., Yuvaraj, M., Jayavel, R. (2018). Synthesis and characterization of binary transition metal oxide/reduced graphene oxide nanocomposites and its enhanced electrochemical properties for supercapacitor applications. Journal of Materials Science: Materials in Electronics, 29(14): 11738-11748. https://doi.org/10.1007/s10854-018-9272-0

[17] Mahanta, R., Chetri, P., Shukla, N., Bora, D. (2024). Daylight photocatalytic activity of SnO_2@ Al_2O_3 core-shell: An experimental & first principles study. Physica B: Condensed Matter, 690: 416230. https://doi.org/10.1016/j.physb.2024.416230

[18] Huang, X., Feng, Y., Bai, C., Wu, K., Ke, J., Xiong, D., He, M. (2020). SnO_2-Al_2O_3-graphite nanosheets as a long-life and high-rate anode material for lithium-ion batteries. Chemical Physics Letters, 749: 137456. https://doi.org/10.1016/j.cplett.2020.137456

[19] Kumar, C., Mishra, N.K., Kumar, A., Bhatt, M., Chaudhary, P., Singh, R. (2016). Structural investigation of nanomixed xSnO_2–Al_2O_3 synthesized by sol–gel

route. Applied Nanoscience, 6(7): 1059-1064. https://doi.org/10.1007/s13204-015-0515-6

[20] Singh, R., Kumar, M., Shankar, S., Singh, R., Ghosh, A.K., Thakur, O.P., Das, B. (2015). Effects of Sb, Zn doping on structural, electrical and optical properties of SnO_2 thin films. Materials Science in Semiconductor Processing, 31: 310-314. https://doi.org/10.1016/j.mssp.2014.12.010

[21] Sadeghzadeh-Attar, A. (2020). Binary Zn-doped SnO_2/Al_2O_3 nanotube composites for visible-light-driven photocatalytic degradation of basic blue 41. ACS Applied Nano Materials, 3(10): 9931-9942. https://doi.org/10.1021/acsanm.0c01939

[22] Jabeen, A., Rahman, S.U., Shah, A., Khan, S.U., et al. (2025). Tailoring novel SnO2/α-MnO2 composites for photocatalytic performance under visible-light. Arabian Journal for Science and Engineering, 50(9): 6459-6470 . http://doi.org/10.1007/s13369-024-09406-7

[23] Monga, K., Aggarwal, M., Singh, V., Chaudhary, S. (2024). Zinc and [Zinc, Nickel]: Co doped SnO2 nanoparticles as prospective electron transport layer materials for efficient lead free-MASnI3 perovskite solar cells. Chemical Physics Impact, 8: 100651 . https://doi.org/10.1016/j.chphi.2024.100651

[24] Dhawale, V.P., Khobragade, V., Kulkarni, S.D. (2018). Synthesis and characterization of aluminium oxide (Al2O3) nanoparticles and its application in azodye decolourisation. Chemistry, 27: 31. https://doi.org/10.11648/j.ijec.20180201.13

[25] Guo, X., Qing, Y., Wu, Y., Wu, Q. (2016). Molecular association of adsorbed water with lignocellulosic materials examined by micro-FTIR spectroscopy. International Journal of Biological Macromolecules, 83: 117-125. https://doi.org/10.1016/j.ijbiomac.2015.11.047

[26] Guo, X., Yuan, H., Xiao, T., Wu, Y. (2019). Application of micro-FTIR spectroscopy to study molecular association of adsorbed water with lignin. International Journal of Biological Macromolecules, 131: 1038-1043. https://doi.org/10.1016/j.ijbiomac.2019.03.193

[27] González, E.Q., Medina, E.L., Robles, R.V.Q., Gálvez, H.E.G., et al. (2022). A study of the optical and structural properties of SnO_2 nanoparticles synthesized with Tilia cordata applied in methylene blue degradation. Symmetry, 14(11): 2231. https://doi.org/10.3390/sym14112231

[28] Giridasappa, A., Shareef, M.I., Gopinath, S.M., Rangappa, D., Shivaramu, P.D., Sabbanahalli, C. (2023). Synthesis, antioxidant, bactericidal and antihemolytic activity of Al_2O_3 and SnO_2 nanoparticles. Proceedings of the National Academy of Sciences, India Section B: Biological Sciences, 93(4): 871-882. https://doi.org/10.1007/s40011-023-01444-9

[29] Pourmadadi, M., Hafezi, A.R., Mafirad, S., Nouri, M., et al. (2025). Development and evaluation of SA/PVP/γ-Al_2O_3 nanocarriers for targeted delivery of curcumin in colon cancer therapy. Journal of Drug Delivery Science and Technology, 105: 106632. https://doi.org/10.1016/j.jddst.2025.106632

[30] Tański, T., Smok, W., Matysiak, W. (2021). Characterization of morphology and optical properties of SnO_2 nanowires prepared by electrospinning. Bulletin of the Polish Academy of Sciences. Technical Sciences, 69(5): 1-8. http://doi.org/10.24425/bpasts.2021.137507

[31] Ghrib, B., Slama, S.S.B., Dimassi, W., Gaidi, M., Ouertani, R. (2021). Effect of Al_2O_3 coatings on microstructural and optoelectronic properties of porous Si/SnO_2 composites. https://doi.org/10.21203/rs.3.rs-670960/v1

[32] Caputo, F., Clogston, J., Calzolai, L., Rösslein, M., Prina-Mello, A. (2019). Measuring particle size distribution of nanoparticle enabled medicinal products, the joint view of EUNCL and NCI-NCL. A step by step approach combining orthogonal measurements with increasing complexity. Journal of Controlled Release, 299: 31-43. https://doi.org/10.1016/j.jconrel.2019.02.030

[33] Jayachandran, V., Dhandapani, V.S., Muniappan, E., Park, D., Kim, B., Arun, A.P., Ayyappan, P.R. (2022). Assessment of the synergetic performance of nanostructured CeO_2-SnO_2/Al_2O_3 mixed oxides on automobile exhaust control. Materials, 15(23): 8460. https://doi.org/10.3390/ma15238460

[34] Oliveira, M.L., Da Boit, K., Schneider, I.L., Teixeira, E.C., Borrero, T.J. C., Silva, L.F. (2018). Study of coal cleaning rejects by FIB and sample preparation for HR-TEM: Mineral surface chemistry and nanoparticle-aggregation control for health studies. Journal of Cleaner Production, 188: 662-669. https://doi.org/10.1016/j.jclepro.2018.04.050

[35] Zhu, S., Liu, J., Sun, J. (2019). Precise growth of Al_2O_3/SnO_2/CNTs composites by a two-step atomic layer deposition and their application as an improved anode for lithium ion batteries. Electrochimica Acta, 319: 490-498. https://doi.org/10.1016/j.electacta.2019.07.027

[36] Hussein, S.A., Gehad, S.M., Ebnalwaled, A.A. (2023). Effect of metal oxides ratio on the properties of SnO_2/Al_2O_3 nanocomposites. IOSR Journal of Applied Physics, 14(1): 52-59. https://doi.org/10.9790/4861-1404015259

[37] Kim, Y.E., Lee, W., Youn, M.H., Jeong, S.K., Kim, H.J., Park, J.C., Park, K.T. (2019). Leaching-resistant SnO_2/γ-Al_2O_3 nanocatalyst for stable electrochemical CO_2 reduction into formate. Journal of Industrial and Engineering Chemistry, 78: 73-78. https://doi.org/10.1016/j.jiec.2019.05.042

[38] Rodriguez, R., Müller, S., Colombeau, L., Solier, S., Sindikubwabo, F., Cañeque, T. (2025). Metal ion signaling in biomedicine. Chemical reviews, 125(2), 660-744. https://doi.org/10.1021/acs.chemrev.4c00577

[39] Singer, L., Karacic, S., Szekat, C., Bierbaum, G., Bourauel, C. (2023). Biological properties of experimental dental alginate modified for self-disinfection using green nanotechnology. Clinical Oral Investigations, 27(11): 6677-6688. https://doi.org/10.1007/s00784-023-05277-8

[40] Mukhanu, C. (2023). Screening of natural compounds inhibiting biofilm formation by antibiotic resistant enterobacteria using experimental trials and computational molecular modelling (Master's thesis, University of Pretoria (South Africa)).

[41] Díez-Pascual, A.M., Díez-Vicente, A.L. (2016). PEGylated boron nitride nanotube-reinforced poly (propylene fumarate) nanocomposite biomaterials. RSC Advances, 6(83): 79507-79519. https://doi.org/10.1039/C6RA09884C

[42] Garg, D., Chatterjee, T. (2023). A case of profound hypertriglyceridemia causing

pseudohypobicarbonatemia. Cureus, 15(4): e37489. https://doi.org/10.7759/cureus.37489
[43] Yao, Z., Wu, D., Liu, J., Wu, W., Zhao, H., Tang, J. (2017). Recycling of typical difficult-to-treat e-waste: Synthesize zeolites from waste cathode-ray-tube funnel glass. Journal of Hazardous Materials, 324: 673-680. https://doi.org/10.1016/j.jhazmat.2016.11.041
[44] Mammari, N., Lamouroux, E., Boudier, A., Duval, R.E. (2022). Current knowledge on the oxidative-stress-mediated antimicrobial properties of metal-based nanoparticles. Microorganisms, 10(2): 437. https://doi.org/10.3390/microorganisms10020437
[45] Zhang, J., Chen, Z., Chen, Q. (2024). Advanced nano-drug delivery systems in the treatment of ischemic stroke. Molecules, 29(8): 1848. https://doi.org/10.3390/molecules29081848
[46] Franco, D., Calabrese, G., Guglielmino, S.P.P., Conoci, S. (2022). Metal-based nanoparticles: Antibacterial mechanisms and biomedical application. Microorganisms, 10(9): 1778. https://doi.org/10.3390/microorganisms10091778
[47] Swartjes, J.J., Sharma, P.K., Kooten, T.V., van der Mei, H.C., Mahmoudi, M., Busscher, H.J., Rochford, E.T. (2015). Current developments in antimicrobial surface coatings for biomedical applications. Current Medicinal Chemistry, 22(18): 2116-2129. https://doi.org/10.2174/0929867321666140916121355
[48] Brandelli, A. (2024). Nanocomposites and their application in antimicrobial packaging. Frontiers in Chemistry, 12: 1356304. https://doi.org/10.3389/fchem.2024.1356304